Comparison of Thermal and Optical Electron-Transfer Barriers in Ruthenium Redox Polyether Melts

Srikanth Ranganathan and Royce W. Murray*

Kenan Laboratories of Chemistry, University of North Carolina, Chapel Hill, North Carolina 27599

Received: August 16, 2004; In Final Form: September 23, 2004

Combining redox active moieties with polyether oligomers produces amorphous, highly viscous, room-temperature molten materials notable for their high concentrations of redox sites that in mixed valent form exhibit facile electron-transfer chemistry. This paper describes experimental determinations and comparison of thermal and optical energy barriers for electron transfers in a specific redox polyether melt, namely the metal complex $Ru(bpy350)_2(CN)_2$ where bpy350 is 4,4′-dimethyl-2,2′-dipyridyl alkyl-bonded to 350 MW polyethylene glycol monomethyl ether. Electrochemical measurements provide apparent electron self-exchange rate constants (k_{EX}) within the Ru(III/II) form of the melt and physical diffusion rates of perchlorate ion (D_{ClO4}), along with the associated thermal activation barrier energies. Plasticization by CO_2 induced swelling of the melt results in enhanced mass and charge transport rates and decreasing energy barriers for both. Optical spectra of the same, electrochemically generated, mixed valent melt display an absorbance interpreted as an intermolecular Ru(II→III) intervalence charge transfer band. The energy barrier results show that the observed thermal electron transfer energy barrier is only an apparent one, being instead controlled by ion atmosphere relaxation processes, whereas the optical energy barrier corresponds to that of the actual electron-transfer process itself.

Introduction

Redox active compounds do not readily form solid solutions of their mixed valent oxidation states, but can be converted into amorphous, semisolid, concentrated room temperature molecular melts from which mixed valent melts can be generated by electrochemical or chemical reactions. The conversion involves covalently attaching polyether oligomers to either the redox species or its counterions.[1] These hybrid redox polyether melts have served as models for studies of charge and mass transport in semisolid environments[1,2] that seek a broader understanding of the factors controlling electron transfers in such environments.

When a weakly coupled, valence-localized mixed-valent system is created (Robin and Day Class II system[3]), electron self-exchange reactions between the donor−acceptor pair can occur by thermal activation, or can be induced optically. Marcus theory presents a theoretical framework for analysis of the thermal electron-transfer process; Hush theory relates optically induced electron transfers to thermal electron transfers.[4,5] Given the strong interplay between theory and experiment in these kinds of electron transfers, comparisons of their properties in binuclear mixed-valent systems have been actively pursued.[6] It has been classically difficult, because of experimental limitations and the lack of suitable model compounds, to examine *both* optical and thermal electron transfers for the same donor−acceptor system. Hybrid redox polyether melts provide opportunities to access such data. When a mixed-valent system is generated in the melt, the inherently high concentration of donor−acceptor sites results in voltammetric currents dominated by the rates of thermally activated electron self-exchanges, and optical absorbances corresponding to intermolecular charge transfers.[7a] The thermal barrier energy ($E_{A,ET}$) is predicted, in the simplest case, from the optical energy (E_{OP}) of the intervalence charge-transfer band (IVCT):[4]

$$E_{A,ET} = \frac{E_{OP}}{4} \quad (1)$$

This was explored by Ritchie et al.[7] for melts based on ruthenium complexes, finding that in the three melts probed, the thermal barriers (19−30 kJ/mol) predicted from optical data with eq 1 were much smaller than the experimental thermal barrier energies (47−71 kJ/mol). Our understanding of the origin of the large thermal barriers was incomplete at the time, and this comparison was not immediately fruitful. Further investigation of other redox polyether melts has since produced an improved picture of the thermal processes,[2] namely by finding a strong correlation between the rates and thermal barriers of homogeneous electron self-exchanges (k_{EX}) and counterion mass transport (D_{ClON}). The interpretation is that thermally activated electron-transfer dynamics are dominated by an ion atmosphere reorganization process, and not by the intrinsic rate of the electron-transfer event.[2] The present comparison of optical and thermal electron-transfer processes was initiated based on this new understanding of the thermal process.

This report describes the synthesis of a new ruthenium complex melt, $Ru(bpy350)_2(CN)_2$, where the polyether oligomers are attached covalently to the dipyridyl ligand through an alkyl linkage, and a comparison of the optical and thermal electron-transfer barrier energies in this melt as well as those studied by Ritchie et al.[7] $LiClO_4$ was dissolved in the melt for ionic conductivity. Voltammetry of the Ru(II/III) couple in the $Ru(bpy350)_2(CN)_2$ melt gave thermally activated apparent electron self-exchange rate constants (k_{EX}); ionic conductivity measurements gave physical diffusion coefficients of perchlorate ion (D_{ClO_4}). The activation barriers of both were obtained in vacuo and at different pressures in a plasticizing CO_2 bath, and as in preceding investigations, proved to be similar, consistent with ion atmosphere control of the electron-transfer rate. Optical

10.1021/jp046310b CCC: $27.50
Published on Web 12/02/2004

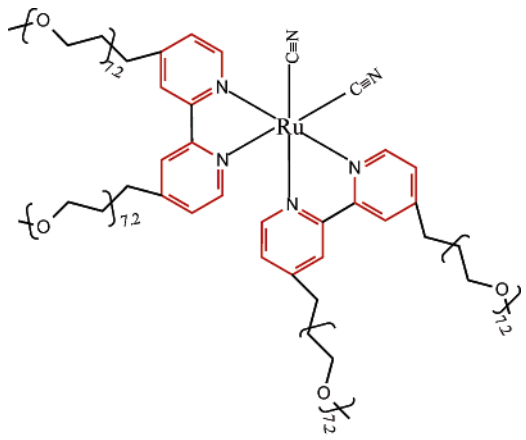

$Ru(bpy350)_2(CN)_2$

spectra revealed a Ru(II→III) IVCT band in an electrochemically generated Ru(III/II) mixed-valent melt. Examination of optical data for the new and previous[7] ruthenium IVCT bands yields a good consensus between predicted and observed E_{OP} values, from which we infer that the optical data reveal properties of the intrinsic electron-transfer event. The optical measurements provide a guide for future studies of electron-transfer dynamics in the relatively unexplored semisolid-state environment.

Experimental Section

Reagents. Polyethylene glycol monomethyl ether with average molecular weight (M_n) 350 (MePEG, Aldrich) was dried under vacuum at 70 °C for at least 24 h before use. 4,4′-Dimethyl-2,2′-dipyridyl (bpy, Aldrich) was purified by sublimation. Tetrahydrofuran (THF, Aldrich) was freshly distilled over dry sodium metal. Cobalticinium$^+$ $MePEGSO_3^-$ (CoCp melt) and ferrocene-CH_2-$N(CH_3)_3^+$ $MePEGSO_3^-$ (Fc melt) were available from previous synthesis.[8]

Synthesis of bpy Ligand with Two Tails (bpy350). The MePEG was tosylated as described before.[9a] The two alkyl groups of bpy were deprotonated with lithium diisopropyl amide and then reacted with tosylated MePEG to give the bi-tailed ligand, bpy350, as detailed elsewhere.[9b] The product was extracted with acid (10% HCl) and neutralized with 2 M KOH, and the neutralized solution was extracted with methylene chloride (CH_2Cl_2). The resulting yellow oil was further purified with column chromatography as previously described[9b] except for minor changes in the eluent. The column was initially washed with CH_2Cl_2 followed by elution with 2% and then 4% methanol in CH_2Cl_2 to obtain bi-tailed bpy350. The eluent from 2% methanol contained significant amounts of mono-tailed bpy350, which was not used further. The 4% methanol eluent contained >80% of bi-tailed product and was used without further purification.

Synthesis of Complex. $Ru(bpy350)_2(CN)_2$ was prepared by using previously reported procedures, replacing dipyridyl with bpy350.[10] The initial oxalato complex, $Ru(bpy350)_2(C_2O_4)$, was extracted with CH_2Cl_2 from the reaction mixture until the CH_2Cl_2 layer developed no purple color. The CH_2Cl_2 layer was dried with sodium sulfate and filtered, and solvent was removed under vacuum. The oxalato complex was not further purified and was reacted as such with KCN to prepare $Ru(bpy350)_2(CN)_2$. After reaction with KCN, the reaction mixture was extracted repeatedly with CH_2Cl_2 until the CH_2Cl_2 layer developed no reddish orange color. CH_2Cl_2 was removed under vacuum and further purification was achieved by using silica gel column with methanol eluent. The orange middle fraction was found to contain the required complex as judged by UV−visible spectroscopy.[11] UV−vis λ_{max} in acetonitrile: 292, 341, 492 nm.

Electrochemical Measurements. Electrochemical studies of the metal complex melts were conducted as before with use of a locally built low-current potentiostat with computer control.[12] The microelectrode cell consisted of tips of four wires exposed in an insulating platform: a 25 μm diameter Pt wire working electrode; a 0.5 mm diameter Ag wire quasi-reference electrode; and two 0.4 mm diameter Pt wire electrodes, one of which is used as an auxiliary electrode for voltammetry and chronoamperometric measurements while both were used for ionic conductivity measurements. This electrode fabrication and its use in a high-pressure cell container have been detailed before by Lee et al.[2a,b] The end of the assembly was hand polished successively with 1, 0.3, and 0.05 μm alumina (Buehler)−Nanopure water (Barnsted) slurries on a Buehler microcloth polishing cloth. The working electrode was electrochemically cleaned in 0.5 M H_2SO_4 followed by drop-casting a layer of the metal complex melt from a solution, with supporting electrolyte, in acetonitrile. The resulting melt films have a thickness >100 μm. The microelectrode radius, calibrated with ferrocene solution in acetonitrile, was found to be 14 μm.[13]

Cyclic voltammetry, chronoamperometry, and ionic conductivity measurements on $Ru(bpy350)_2(CN)_2$ melt with 1.0 M $LiClO_4$ added as supporting electrolyte were performed at several temperatures in vacuum and at different CO_2 pressures. Small amounts (~2.5 mol equiv) of MePEG were also added to the Ru melt to provide voltammetric stability. Drop-cast films of melts were dried under vacuum (~1×10^{-3} Torr) at 60 °C for at least 48 h before commencing electrochemical studies. The film was equilibrated at each temperature and pressure for at least 1 h before recording the data. Chronoamperometric measurements involved 300−400 mV potential steps (determined by cyclic voltammetry before each potential step) from a potential just before the Ru(III/II) wave to a diffusion-limited Ru(III/II) potential past the peak. The data were collected for 2 min and analyzed by both Cottrell and Shoup−Szabo equations,[14] using SigmaPlot software (SPSS Inc.); the reported values are averages of these.

Ionic conductivity measurements were accomplished on the same films as above with a Solartron Model SI 1260 impedance analyzer−SI 1287 electrochemical interface. Impedance measurements in the frequency range from 1 MHz to 1 Hz were performed at a dc bias of 0 V while the ac amplitude was set to 300 mV. The resistance of the melt was obtained from the low-frequency real-axis intercept of the complex impedance semicircle. The geometric cell constant was found to be 16.74 cm^{-1} by using conductivity calibration standards (Fisher Scientific) for the microelectrode assembly.

Spectroelectrochemical Measurements. The spectroelectrochemical thin layer cell contained a small amount of dried Ru melt with 1.0 M $LiClO_4$ supporting electrolyte, sandwiched between two 25 mm × 75 mm indium-coated tin oxide slides (ITO, Delta Technologies, MN) separated by a ~50 μm thick Monokote (Topflight, Great Plains Model Distribution, IL; sky blue color) spacer (see Supporting Information Figure S-I), and the conductive sides of the ITO plates were exposed to the melt and the slides were slightly offset along the long axis for electrical connections. The filled cell was sealed with TorrSeal (Vacuum Technologies) and placed in the beam-path of a BioRad FT1600 series NIR/IR spectrometer. Any area not exposed to the incident beam was masked. A potential difference (ΔE) was applied between the two ITO slides, using a Pine

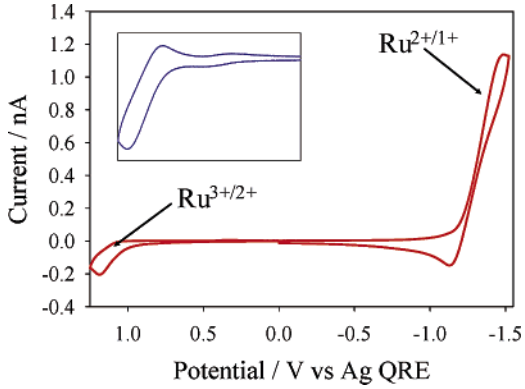

Figure 1. Cyclic voltammogram (100 mV/s) of neat $Ru(bpy350)_2(CN)_2$/1.0 M $LiClO_4$ melt showing both Ru(III/II) and Ru(II/I) waves. The inset shows the Ru(III/II) voltammogram of $Ru(bpy350)_2(CN)_2$ melt with 2.5 mol equiv of MePEG added/1.0 M $LiClO_4$, both at 23 °C under vacuum on a 14-μm Pt microelectrode.

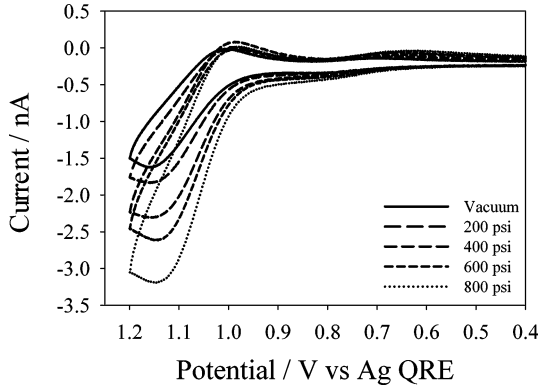

Figure 2. Cyclic voltammograms (100 mV/s) of $Ru(bpy350)_2(CN)_2$ melt with 2.5 mol equiv of MePEG added/1.0 M $LiClO_4$ at 23 °C and at the indicated CO_2 pressures.

RDE4 potentiostat; a slow-scan (2 mV/s) cyclic voltammogram (BAS100B potentiostat, Bioanalytical System, West Lafayette, IN) identified the required ΔE. It was observed that prolonged application (>60 min) of $\Delta E > 2$ V damaged the melt (gas bubbles and change in melt color from red to dark brown) limiting the duration of such experiments. A spectrum of the initial melt was used as the background; it showed no specific features in the region of interest, except for solvent and ITO peaks.

Spectroelectrochemistry of 1:1 mol:mol mixtures of the $[Ru(bpy350)_2(CN)_2]$ melt and either $[Cp_2Co^+][MePEG_{350}SO_3^-]$ or $[Cp_2Fe\text{-}CH_2\text{-}N(CH_3)_3^+][MePEG_{350}SO_3^-]$ melt was conducted in a similar manner.

Results and Discussion

Measurements of Thermal Activation of Electron Transfer and Counterion Transport. *Electron Transfer.* Figure 1 shows the cyclic voltammetry of a neat $Ru(bpy350)_2(CN)_2$ metal complex melt under vacuum. Because this metal complex is neutral (unlike other metal polypyridine complexes that we have studied[1d−f,2d,7b]), 1.0 M $LiClO_4$ is added for ionic conductivity. As seen before,[1d] although the same metal complex physically diffuses during both oxidation and reduction, currents for Ru(II/I) reduction ($[Ru(bpy350)_2(CN)_2]^{0/1-}$) exceed those for Ru(III/II) oxidation ($[Ru(bpy350)_2(CN)_2]^{1+/0}$) owing to larger electron-transporting self-exchange rate constants for the Ru(II/I) reaction. The melt voltammetry in Figure 1 was not stable in repeated scans over the Ru(II/I) and Ru(III/II) waves, currents gradually diminishing. The instability was corrected by adding small amounts of MePEG to the melt as a plasticizer; electrochemical responses were then stable over extended periods of observation. Further experiments were performed with the addition of 2.5 mol equiv of MePEG to the $Ru(bpy350)_2(CN)_2$ melts.

Sorption[2a,b] of CO_2 into redox polyether hybrids increases voltammetric charge and mass transport rates and thus serves as a convenient plasticizing tool for systematic variation of melt fluidity. The (stable) voltammetry in Figure 2 shows that Ru(III/II) currents steadily increase with increasing CO_2 pressure from vacuum to 800 psi. This change is quantitatively reversible. Like Co complex melts,[2a,b] the current increase is not simply pressure induced but instead reflects plasticization induced by CO_2 sorbed into the melt. The partitioned CO_2 swells the melt matrix and enhances its free volume. The increasing currents in Figure 2 are thus attributed to plasticization by CO_2 sorbed into the $Ru(bpy350)_2(CN)_2$ melt/$LiClO_4$ mixture. The charge transport diffusion rate in the melt, D_{APP}, is measured with chronoamperometry.

According to the cubic lattice model of the Dahms−Ruff formulation,[15] D_{APP} is a summation of the physical diffusion coefficient (D_{PHYS}) of the metal complex and the rate of electron hopping as reflected in the electron diffusion coefficient D_E,

$$D_{APP} = D_{PHYS} = D_E = D_{PHYS} + \frac{k_{ex}\delta^2 C}{6} \qquad (2)$$

where k_{EX} is the apparent self-exchange rate constant (M^{-1} s^{-1}), δ is the equilibrium metal complex center-to-center distance (cm), and C is the metal complex concentration (M). We have generally observed in redox polyether melts that $D_{PHYS} \ll D_E$, so that the contribution of D_{PHYS} to D_{APP} is small (~5%).[1,2] Assuming that this is also true for the present 4-PEG-tailed complex $Ru(bpy350)_2(CN)_2$ is reasonable considering the prior evidence[1d] that, in relation to 6-PEG-tailed complexes (in which typically $D_{APP} \gg D_{PHYS}$), a diminished polyether PEG-tail content suppresses both charge and mass transport properties of these metal complex melts. Accordingly, we assume D_{PHYS} is negligible in eq 2. Concurrent volume swelling of the melt by sorbed CO_2 was estimated as ca. 20% based on other studies,[16] in order to correct the metal complex concentrations and center-to-center distances (δ). The results are shown in Table 1. The electron diffusion rate D_E and associated apparent electron self-exchange rate constant, k_{EX}, in the melt increase ~10-fold from vacuum to 800 psi of plasticizing CO_2.

Counterion Transport. The physical diffusivity of the ClO_4^- ions (D_{ClO_4}) is estimated from the ionic conductivity of the metal complex melts, using the Nernst−Einstein equation:[1h,17]

$$\sigma_{ION} = \frac{F^2}{RT}[z_{Li}{}^2 D_{Li} C_{Li} + z_{ClO_4}{}^2 D_{ClO_4} C_{ClO_4}] \qquad (3)$$

where σ_{ION} is ionic conductivity ($ohm^{-1}cm^{-1}$), z is the ion's charge, D is the ion diffusion coefficient (cm^2/s), and C is concentration (M). The mass mobility of the ClO_4^- ion is assumed to predominate over that of Li^+ (because of known Li−polyether chain associations[1h,18]) and of the Ru(III) form of the melt metal complex, i.e., ClO_4^- ions are the dominant mobile ions in the melt. Table 1 shows that the D_{ClO_4} values also increase by ~10-fold over the range of CO_2 pressures.

The increase in D_{ClO_4} with CO_2 pressure seen in Table 1 parallels that of D_E and k_{EX}, and the ratio D_{ClO_4}/D_E is more or less constant over the range of CO_2 pressures. It is significant

TABLE 1: Summary of Thermal Data for Ru(III/II) Electron Transfers and Ion Transport in $Ru(bpy350)_2(CN)_2$ Metal Complex Melt, at a Series of CO_2 Pressures[a]

	CO_2 pressure at RT/psi[b]				
	vacuum	200	400	600	800
concn/M[c]	0.47	0.46	0.44	0.43	0.41
δ/Å[d]	15.2	15.4	15.5	15.7	15.9
D_E(24 °C)/cm^2 s^{-1} [e]	1.7×10^{-10}	2.9×10^{-10}	4.9×10^{-10}	8.1×10^{-10}	1.7×10^{-9}
σ_{ion} (24 °C)/ohm^{-1} cm^{-1}	2.6×10^{-6}	6.3×10^{-6}	1.2×10^{-5}	1.9×10^{-5}	3.3×10^{-5}
D_{ClO_4}(24 °C)/cm^2 s^{-1} [f]	7.0×10^{-10}	1.7×10^{-9}	3.3×10^{-9}	5.1×10^{-9}	8.8×10^{-9}
D_{ClO_4}/D_E	4.0	5.8	6.8	6.4	5.2
$E_{A,ET}$/kJ mol^{-1} [g]	47	43	38	33	29
$E_{A,ion}$/kJ mol^{-1} [g]	48	39	33	27	25
k_{ex}(24 °C)/M^{-1} s^{-1} [h]	9.5×10^4	1.6×10^5	2.8×10^5	4.6×10^5	9.6×10^5

[a] The melt contains 2.5 mol equiv of MePEG and 1.0 M $LiClO_4$. [b] Pressure at room temperature, CO_2 density is held constant. [c] Estimated assuming 20% increase in swelling volume from 0 to 1000 psi.[16] [d] Estimated from swelling volume. [e] From chronoamperometry; assuming $D_{PHYS} = 0$. [f] From conductivity data and the Nernst−Einstein equation assuming $D_{Li} = 0$. [g] From slopes for activation plots. [h] Apparent rate constant calculated from D_E values, using Dahms−Ruff eq 2.

and useful that the ratio D_{ClO_4}/D_E exceeds unity, since it means that electronic migration effects—in which electric field gradients in the melts enhance electron hopping rates—are negligible. (In previous studies the ratio was sometimes less than unity, requiring theoretical estimation of a correction for electronic migration[1e,g,h,2a,b,d]). The significance of the parallel variation of D_{ClO_4} and D_E is discussed below.

Thermally Activated Electron-Transfer Barriers. Measurement of D_E and σ_{ION} for the $Ru(bpy350)_2(CN)_2$ melt at different temperatures at each CO_2 pressure yields activation barrier energies of electron transfer and counterion transport. Assuming a symmetrical self-exchange reaction (reaction entropy and entropy of activation are zero), the temperature dependence of electron transfer can be written as[19]

$$k_{EX} = K_P \kappa \nu_N \exp\left[-\frac{\Delta G^*}{RT}\right] \quad (4)$$

where K_P is the precursor formation constant, κ is electron-transmission coefficient, ν_N is nuclear frequency factor, and ΔG^* is enthalpy of activation ($\approx E_{A,ET}$). Figure 3 shows activation plots for D_E and σ_{ION}; the resulting barrier energies are listed in Table 1. We see the striking facts that the barrier energies for D_E and σ_{ION} (and hence D_{ClO_4}) (a) are very similar and (b) decrease as the CO_2 pressures are increased. The decrease in activation barrier reflects plasticization by CO_2, which generally increases mass and charge transport rates in redox polyether melts.[2a,b] The significance of the similarity of the activation barrier energies is related to that of D_{ClO_4} and D_E and is discussed later.

We have considered previously the intercepts of activation plots of ln k_{EX} vs $1/T$ in terms of reaction adiabaticity[1,2] in polyether melt redox systems. The intercepts have supported adiabaticity. However, based on the ion atmosphere relaxation model, we believe that it is no longer meaningful to relate the intercepts to reaction adiabaticity.

Comparison to Ion Atmosphere Relaxation Model. A general outcome of our previous measurements of electron transport in semisolid hybrid redox polyether melts has been that the obtained values of k_{EX} are smaller, and those of $E_{A,ET}$ are larger, than values typical of analogous self-exchange reactions of metal complexes in fluid, dilute solutions or those predicted by Marcus theory.[1d,f−h,19,20] Additionally, the observed $E_{A,ET}$ thermal barriers are larger than those predicted based on optical electron transfers,[7] which is also the case for the $Ru(bpy350)_2(CN)_2$ melt (as reported below).

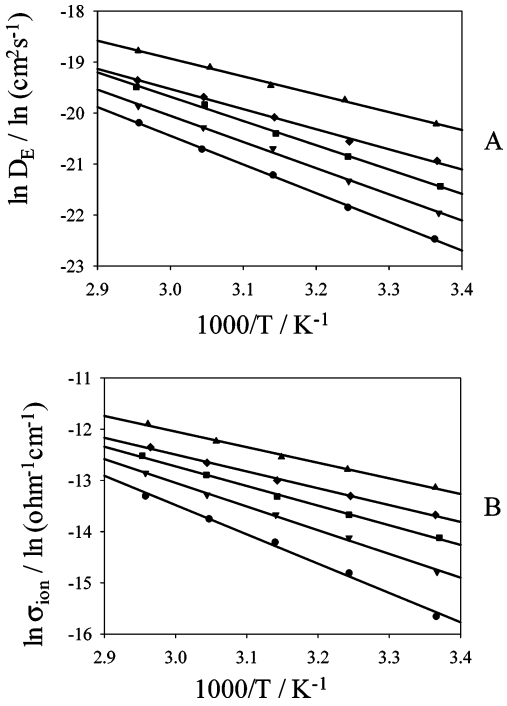

Figure 3. Activation plots of (A) D_E and (B) σ_{ION} at a series of CO_2 pressures: vacuum (●), 200 psi (▼), 400 psi (■), 600 psi (◆), and 800 psi(▲).

At the outset of our investigations of hybrid redox polyether melts, we drew upon an apparent parallel between electron transfer and mass transport rates. Drawing from earlier interpretations of heterogeneous electron-transfer reactions in viscous solutions, a model based on solvent dynamics control was proposed,[1e,g,h] in which values of reactant physical diffusivity (D_{PHYS}) served as barometers of repolarization dynamics in the melts. Recently, however, that interpretation has been challenged[2a−c] by recognition of the importance of relaxation of the ionic atmosphere surrounding electron donor−acceptor reaction partners in the melts. The ion atmosphere relaxation model is based on an analysis[21] of the effects of ion pairing on electron transfers. Note that by virtue of their high concentrations (nearly 0.5 M in the present case) and lack of diluting solvent, the constituents of hybrid redox polyether melts are intrinsically "ion paired".

The ion-pair "electron-transfer first" case[21] is represented by a reversible electron-transfer step (with forward and reverse rate constants, k_1 and k_{-1} respectively, and $K_{EQ} = k_1/k_{-1}$) followed

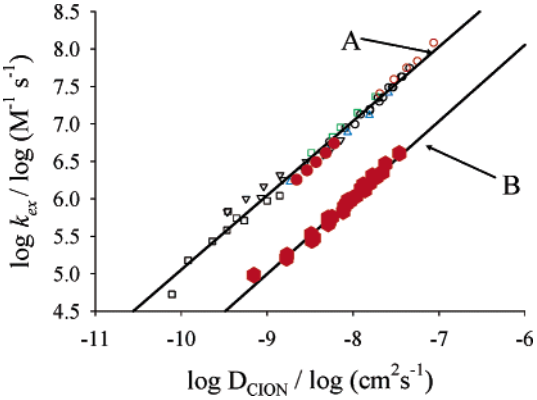

Figure 4. Linear log−log relationship between k_{EX} (M^{-1} s^{-1}) and D_{ClON} (cm^2 s^{-1}) for Co(II/I) and Ru(III/II) electron transfers in redox polyether melts: curve A (open symbols), for Co(II/I) in cobalt tris-bipyridine and tris-phenanthroline melts with different modes of plasticization (reported in ref 20); curve A (●), for Ru(III/II) in $Ru(bpy(CO_2MePEG)_2)_3(ClO_4)_2$ melt;[2d] and curve B (●), for Ru(III/II) (present data) in $Ru(bpy350)_2(CN)_2$ melt with 2.5 mol equiv of MePEG added/ 1.0 M $LiClO_4$ at all temperatures and CO_2 pressures.

by diffusive redistribution of the neighbor counterion(s) with a rate constant k_2:

$$X^-Ru^{3+}Ru^{2+} \underset{k_{-1}}{\overset{k_1}{\rightleftarrows}} X^-Ru^{2+}Ru^{3+} \overset{k_2}{\rightleftarrows} Ru^{2+}Ru^{3+}X^- \quad (5)$$

where in the present case X^- is ClO_4^-. The overall electron-transfer rate constant (k_{EX}) is

$$\frac{1}{k_{EX}} = \frac{1}{k_1} + \frac{k_{-1}}{k_2 k_1} = \frac{1}{k_1} + \frac{1}{k_{EQ}k_2} \quad (6)$$

When the electron-transfer rate constant k_1 is sufficiently large that the far right-hand term in eq 6 is dominant, $k_{EX} = K_{EQ}k_2$, where $k_2 = D_{ClON}(\pi/2a)^2$, and "*a*" is the diffusion length of the relocated ion. In this case, the *net electron-transfer rate is determined by the diffusive counterion dynamics*. That is, the net electron-transfer rate that is calculated from the electron-diffusion coefficient D_E (and its barrier energy $E_{A,ET}$) becomes controlled by the values of D_{ClON} (and its barrier energy $E_{A,ION}$).

The consequences of the above model on interpretation of thermally activated electron self-exchanges in hybrid redox polyether melts are profound. (a) Experimental values of k_{EX} do not measure intrinsic electron-transfer rates, but instead reflect ion transport rates. This is also true for heterogeneous electron transfers at electrode-melt interfaces. (b) Values of electron-diffusion coefficients D_E should be the same as those for counterions (D_{ClO_4}), and $E_{A,ET}$ barrier energies should be the same as those for ion transport ($E_{A,ION}$). (c) Variations of k_{EX} should be accompanied by parallel variations in D_{ClO_4}. (d) The observed k_{EX} values should ideally be independent of the metal in the metal complex. (e) Electron self-exchanges (i.e., transport of charge by electron hopping) should be completely extinguished when the counterion is diffusively immobile. Indeed, all of the above features have been observed,[2a−d] and many are illustrated by the data on curve A in Figure 4. The curve A data were taken in four different investigations, including variations in temperature and modes of plasticization (MePEG and CO_2) and data for Co(II/I) and Ru(III/II) electron transfers in tris-bipyridine complex melts. The slope of the log−log plot is 1.0. The data for the Ru(III/II) tris-bipyridine complex melt, $[Ru(bpy(CO_2MePEG)_2)_3](ClO_4)_2$, in Figure 4 are previously unpublished and further details will be presented elsewhere.[2d]

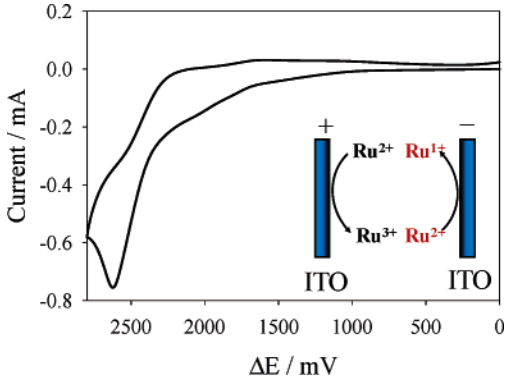

Figure 5. Slow scan (2 mV/s) cyclic voltammogram of $Ru(bpy350)_2(CN)_2$ melt with 2.5 mol equiv of MePEG and/1.0 M $LiClO_4$ in a thin layer cell with ITO electrodes. The inset shows a cartoon of Ru^{2+} oxidation on anode (+) and Ru^{2+} reduction on cathode (−) ITO electrodes.

The $Ru(bpy350)_2(CN)_2$ melt results in Table 1 conform to the ion atmosphere relaxation model's tenants: similar D_E and D_{ClO_4}, and similar $E_{A,ET}$ and $E_{A,ION}$. Figure 4, curve B, shows a log−log plot of k_{EX} and D_{ClO_4}; the data form a smooth correlation with a slope of 1.0. The $Ru(bpy350)_2(CN)_2$ melt results are displaced, however, from the correlation among previous data (curve A). According to eq 6, this could occur either through differences in the equilibrium constant of the electron transfer, K_{EQ}, or in the ion diffusive relocation distance "*a*". The $Ru(bpy350)_2(CN)_2$ complex differs from the $M(bpy)_3^{2+}$ complexes in being a less highly charged reaction pair (0/1+) and in being spatially asymmetrical. The former could lead to differences in K_{EQ} and the latter to differences in "*a*" between $Ru(bpy350)_2(CN)_2$ and $M(bpy)_3^{2+}$ complexes. These differences need not be large to account for the displacement effect in Figure 4. For example, assuming a K_{EQ} for the $Ru(bpy350)_2(CN)_2$ electron transfer that is 30% of the value for the other complexes would cause curves A and B to overlay one another exactly.[22] Alternatively, if the chosen value of "*a*" were closer to the Ru-CN/NC-Ru spacing (8.6 Å) than a Ru-bpy/bpy-Ru spacing (15 Å), the curve for $Ru(bpy350)_2(CN)_2$ would move closer to curve A (K_{EQ} will have to be ~0.4 for an exact match). The separation between curves A and B in Figure 4 thus has plausible origins. We believe these are straightforward explanations of Figure 4, and do not override the commanding facts of similar D_E and D_{ClO_4}, and similar $E_{A,ET}$ and $E_{A,ION}$, for the $Ru(bpy350)_2(CN)_2$ metal complex melt.

Optically Induced Electron Transfers. *Spectral Measurements.* Next we seek optical absorbance evidence—an intervalence charge-transfer band—for intermolecular Ru(II→III) electron transfers in a mixed valent $Ru^{III/II}(bpy350)_2(CN)_2$ melt. The mixed valent melt was (in most experiments) generated electrochemically in an optically transparent thin layer electrode cell (Figure S-I). Figure 5 shows a slow potential scan cyclic voltammogram of $Ru(bpy350)_2(CN)_2$ melt (again with added MePEG and 1.0 M $LiClO_4$) in the thin layer cell. At a potential bias between the transparent electrodes approximately equaling the difference in the formal potentials of the Ru(III/II) and Ru(II/I) reactions of the metal complex (Figure 1), a current peak appears that corresponds to concurrent Ru(II) oxidation at one electrode and reduction at the other. In this and other spectroelectrochemical measurements, electrolysis to mixed valent materials is far from complete (currents and ensuing spectra are not steady state), owing to a combination of the slow charge transport and melt instability that limited the electrolysis time to about 60 min. This electrochemically induced disproportion-

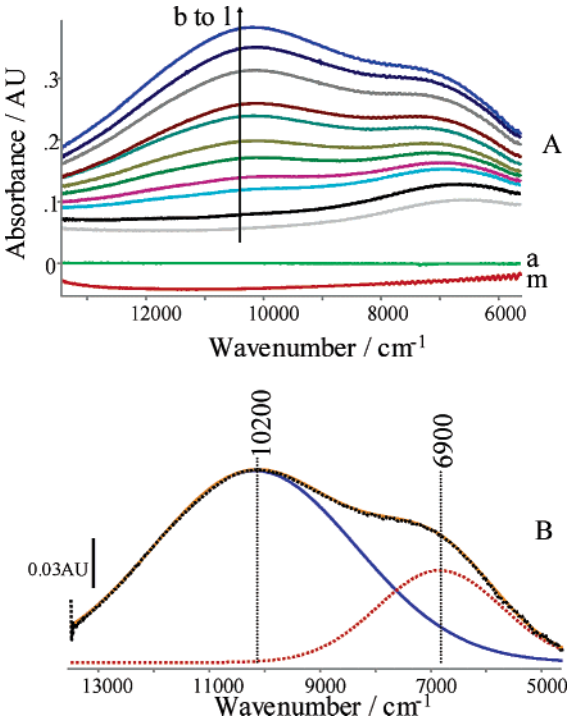

Figure 6. (A) Time-dependent changes in NIR spectra (*b* to *l*) of $Ru(bpy350)_2(CN)_2$ melt in a thin layer cell, after applying a ΔE of 2.6 V: spectrum *a* is the initial melt spectrum before applying any potential; spectrum *m* is the final spectrum taken after 72 h of applying $\Delta E = 0$ V after completing the 2.6 V study. (B) Gaussian curve fits to 2.6 V; 60 min spectrum (spectrum *l* from above) showing two peaks.

ation nonetheless generates layers of mixed valent Ru(III/II) and Ru(II/I) at the facing electrodes.

Spectroelectrochemical measurements involve applying a fixed potential bias ΔE and observing emerging NIR absorbance features. An impurity current peak in Figure 5 at $\Delta E \approx 2.0$ V was checked by applying that potential in one experiment, producing an absorbance band that rises with time at ~6500 cm^{-1} (Supporting Information, Figure S-II). Application of $\Delta E \approx 2.6$ V to activate the primary disproportionation reaction produced, on the other hand, over a 60-min electrolysis, the spectral evolution in Figure 6A, of a band at ~10 000 cm^{-1} as well as at ~6 500 cm^{-1}. The latter is due to the impurity feature mentioned above. Generation of the spectral features in Figures S-II and 6A was reversible; returning the applied potential bias to $\Delta E = 0$ V (regenerating the Ru(II) state) caused the spectrum to return to the original baseline (compare curves *a* and *m* in Figure 6A). Further, chemical oxidation of a $Ru(bpy350)_2(CN)_2$ melt (with bromine) generates similar absorbance features (Figure S-III) that appear during partial oxidation but then disappear as oxidation to an all-Ru(III) melt is completed. The 10 000 cm^{-1} absorbance band in Figure 6 is thereby confirmed as an intervalence charge-transfer feature.

The Figure 6A spectrum was fitted with Gaussian curves; Figure 6B is the result and shows two bands, centered at 6 900 and 10 200 cm^{-1}. [23] A very approximate[24] ϵ of 310 M^{-1} cm^{-1} and an electronic coupling constant of ~160 cm^{-1} are obtained from the peak at 10 200 cm^{-1}. These values are similar to those in a previous study of intra- and intermolecular electron transfers in (chemically generated) mixed valent Ru polyamine complex melts.[7a] Assignment of the absorbance feature in the previous work[7a] was straightforward since only one mixed-valent pair (Ru(III/II)) was present. In the present case, both Ru(III/II) and Ru(II/I) mixed-valent pairs are generated. Assignment was accomplished by disproportionation of 1:1 mole:mole mixtures of the $Ru(bpy350)_2(CN)_2$ complex melt with two other melts that are respectively reduced and oxidized more readily than the Ru(II/I) and Ru(III/II) reactions. Thus, in the $Ru(bpy350)_2(CN)_2$/CoCp melt mixture, application of the appropriate (disproportionating) ΔE, generating Ru(III/II) and Co(II/I) mixed-valent pairs at the facing electrodes, produced a two-band spectrum (Figure S-IV) similar to that in Figure 6A. Neither of these two bands (Figure S-V) appeared upon disproportionating electrolysis of the $Ru(bpy350)_2(CN)_2$/Fc melt mixture, where Ru(II/I) and Fe(III/II) mixed-valent pairs are generated. These results show that the absorbance band at 10 200 cm^{-1} seen upon disproportionation of the pure $Ru(bpy350)_2(CN)_2$ melt is an intermolecular Ru(II→III) intervalence charge transfer, i.e., the $[Ru(bpy350)_2(CN)_2)]^{1+/0}$ couple.

Analysis of Optical Results. We turn to comparison of experimental optical electron-transfer results to theory. Results from both the current $Ru(bpy350)_2(CN)_2$ melt and from a previous Ru polyammine melt complex study[7a] will be considered.

For valence-localized (weakly coupled) mixed-valent systems, the observed optical energy (E_{OP}) for IVCT is given by:[6]

$$E_{OP} = \lambda_{OUT} + \lambda_{IN} + \Delta G^\circ \qquad (7)$$

where λ_{OUT} and λ_{IN} are the outer- and inner-sphere reorganization energies and ΔG° is any additional energy associated with asymmetry of the reactant pair. For electron self-exchanges, ΔG° is ideally zero, but asymmetry can be induced by differential ion-pairing (vide infra). λ_{OUT} can be estimated from the dielectric continuum model,[4] where for reactants with similar radii *r*, one has

$$\lambda_{OUT} = \frac{N(\Delta e)^2}{4\pi\epsilon_0}\left(\frac{1}{r} - \frac{1}{d}\right)\left(\frac{1}{D_{OP}} - \frac{1}{D_S}\right) \qquad (8)$$

where *d* is the distance between the two reactants, D_{OP} and D_S are optical and static dielectric constants of the "solvent" (taken for MePEG in our case; $D_{OP} = 2.128$ and $D_S = 9.16$),[1d] and the other symbols have their usual meaning. The λ_{IN} values in eq 7 are not expected to be much different from previously reported values[6c] and are used as such, except for $Ru(bpy350)_2(CN)_2$ for which λ_{IN} is assumed to be 15 kJ/mol. Table 2 lists the ruthenium complex melt systems studied here and previously,[7a] and calculated values of λ_{OUT} and E_{OP}, assuming $\Delta G^\circ = 0$. Except for $Ru(bpy350)_2(CN)_2$, there is fair agreement (within 20 kJ/mol) between the calculated and observed E_{OP} values. For the intermolecular electron transfers of $Ru(NH_3)_6$ and $Ru(NH_3)_5Py$, the agreement is excellent. The general agreement for the results in semisolid media contrasts with previous studies finding that dielectric continuum theory is inadequate to explain observed E_{OP} for bridged decammine systems.[6c,25]

The mixed-valent $[Ru(bpy350)_2(CN)_2]^{1+/0}$ melt differs from the other melts in at least two important respects: (a) the metal bears a mixture of small (CN) and large (bpy) ligands (b) and the MePEG chain is attached to a ligand (as opposed to the counterion, $MPEG_{350}SO_3^-$, as was the case for the other melts[7a]). The average (density-derived) radius of the $Ru(bpy350)_2(CN)_2$ complex is 6.6 Å, but the short CN ligand and the openness of the bpy ligands allows solvent penetration, and the effective radius of the metal centers[6c] may be much smaller. This is a known problem; for example, calculated E_{OP} values for bridged $(bpy)_2ClRu$-bpy-$Ru(bpy)_2Cl$ complexes are underestimated by ~55 kJ/mol by using an average radius (6.56 Å) that includes the bpy dimension in the calculation,[6c] while an effective radius (4.15 Å) obtained from modeling studies results in an excellent

TABLE 2: Calculated and Optical Electron Transfer Energy Barriers in Ruthenium Polyether Melts

melt system[a]	r,[b] Å	d,[c] Å	λ_{OUT},[d] kJ/mol	E_{OP}(calcd),[e] kJ/mol	E_{OP}(obsd),[f] kJ/mol
$[(NH_3)_5Ru\text{-}pz\text{-}Ru(NH_3)_5]^{+5}$	3.53	6.8	68	85	75
$[(NH_3)_5Ru\text{-}bpy\text{-}Ru(NH_3)_5]^{+5}$	3.87	11.3	85	102	121
$[Ru(NH_3)_6]^{3+/2+}$	3.55	11.8	98	116	109
$[Ru(NH_3)_5py]^{3+2+}$	4.03	11.8	82	99	105
$[Ru(bpy350)_2(CN)_2]^{1+/0}$	6.6	15.2	43	58[g]	122
	(4.3)[h]	(15.2)	(83)	(98)	

[a] Except for $Ru(bpy350)_2(CN)_2$, the melt counterion was $MePEG_{350}SO_3^-$. [b] Radius from ref 6c; for $Ru(bpy350)_2(CN)_2$ the radius is half of the δ of the neat melt. [c] Distance for bridged species from ref 6c and for others based on δ from density measurements. [d] λ_{OUT} calculated by using the dielectric continuum model, eq 8. [e] Calculated by using eq 7, taking λ_{IN} as 17.2 kJ/mol[6c] and $\Delta G° = 0$. [f] Except for $Ru(bpy350)_2(CN)_2$, all data are from ref 7a. [g] λ_{IN} for $Ru(bpy350)_2(CN)_2$ has not been previously reported and is assumed to be 15 kJ/mol. [h] Numbers in parentheses are for an effective radius of 4.3 Å, as explained in the text.

TABLE 3: Calculation of Total Reorganization Energy (λ_{total}), Using the Measured IVCT Bandwidth ($\Delta\nu_{1/2}$), for Ruthenium Polyether Melts (values in parentheses are energies in kJ/mol)

system[a]	expt E_{OP}, cm^{-1} (kJ/mol)	expt $\Delta\nu_{1/2}$, cm^{-1}	calcd[b] $\Delta\nu_{1/2}$, cm^{-1}	λ_{TOTAL},[c] cm^{-1} (kJ/mol)	$\Delta G°$,[d] cm^{-1} (kJ/mol)	% of $\Delta G°$ in E_{OP}
$[Ru\text{-}pz\text{-}Ru]^{5+}$	6300 (75)	1800	3815	1403 (17)	4897 (59)	78
$[Ru\text{-}bpy\text{-}Ru]^{5+}$	10100 (121)	2000	4830	1732 (21)	8368 (100)	83
$[Ru(NH_3)_5Py]^{2+/3+}$	8800 (105)	2300	4510	2290 (27)	6510 (78)	74
$[Ru(NH_3)_6]^{2+/3+}$	9100 (109)	1800	4585	1403 (17)	7697 (92)	85
$[Ru(bpy350)_2(CN)_2]^{1+/0}$	10200 (122)	4500	4685	8766 (105)	1434 (17)	14

[a] Except for $Ru(bpy350)_2(CN)_2$, all the optical data are from ref 7a. [b] Theoretical values calculated by using $\Delta\nu_{1/2} = (2310E_{OP})^{1/2}$, where E_{OP} is the experimental value. [c] Calculated from the observed bandwidth by using $\lambda = (\Delta\nu_{1/2})^2/2310$. [d] Calculated by using $\Delta G° = E_{OP} - \lambda$.

agreement with experiment. Similar effects are seen with binuclear bridged $Ru(bpy)_2py$ systems.[6c] For the $Ru(bpy350)_2(CN)_2$ melt, using an effective radius of 4.3 Å, near the RuCN/ dimension, gives a calculated $E_{OP} = 98$ kJ/mol, much closer to the observed 122 kJ/mol. Overall, the preceding analysis is strikingly successful in analysis of the experimental results. The remaining differences in Table 2 may reflect that $\Delta G° > 0$ by as much as 20 kJ/mol.

An alternative (but much less successful) analysis relies on the observed IVCT bandwidth ($\Delta\nu_{1/2}$) to estimate the total reorganization energy ($\lambda_{TOTAL} = \lambda_{OUT} + \lambda_{IN}$) from Hush's expression.[5,6]

$$\lambda_{TOTAL} = \frac{(\Delta\nu_{1/2})^2}{2310} \tag{9}$$

Table 3 shows bandwidths $\Delta\nu_{1/2}$ predicted (column 4 from left) from the observed E_{OP} results, and experimental $\Delta\nu_{1/2}$ data (column 3 from left) from which λ_{TOTAL} values are estimated, using eq 9. For the $Ru(bpy350)_2(CN)_2$ melt, the λ_{TOTAL} predicted from the experimental $\Delta\nu_{1/2}$ with use of eq 9, 105 kJ/mol, is reasonably close to the observed 122 kJ/mol E_{OP}, considering the neglect of a possible $\Delta G°$. For the other metal complex melts, on the other hand, because the experimental bandwidths are so narrow, they produce λ_{TOTAL} values that are much smaller than the observed E_{OP}, and would require substantial $\Delta G°$ components in the optical electron transfer, by percentages of E_{OP} indicated in the table. These $\Delta G°$ components greatly exceed any that could be inferred from the analysis of Table 2.

Let us examine the possibilities that the top four Ru complex melts might contain substantial $\Delta G°$ components in their IVCT transitions. They are more highly charged than the $[Ru(bpy350)_2(CN)_2]^{1+/0}$ case, and the MePEG "solvent" (i.e., $MePEG_{350}SO_3^-$) has a moderately low dielectric constant that together with the high melt concentration might provoke strong ionic interactions and nonzero $\Delta G°$. The existence of ionic interactions in hybrid redox polyether melts is known from 10 to 15 kJ/mol shifts in redox potentials[26] and from the effects of added electrolytes on mass transport.[1h] MePEG dilution-induced shifts in IVCT E_{OP} of ~31 kJ/mol to higher energies for the $Ru(NH_3)_5py$ melt have been ascribed to ion-pairing,[7a] but this interpretation has not been supported by any subsequent significant shifts in ligand-to-metal or metal-to-ligand UV−visible charge-transfer absorbance bands of other Ru complex melts upon dilution with MePEG or acetonitrile. Numerous other dilute solution studies report shifts in electron-transfer E_{OP} values accompanying addition of electrolyte;[25,27] the IVCT energy of biferrocene monocation can be shifted as much as 24 kJ/mol,[27f] and ~7 kJ/mol shifts have been seen[27h] with $(NC)_5Fe^{3+}$-bis(pyridyl)-ethylene-$Fe^{2+}(CN)_5^-$. The shifts in E_{OP} are attributed to asymmetric ion-pairing; a counterion initially associated with a high-charge metal center becomes distanced from it following the optical electron transfer, i.e., the product has a higher energy content and $\Delta G° > 0$. The effect is analogous to eq 5.

Given the above, the presence of some level of ion interaction that causes a reaction $\Delta G° > 0$ is rather likely, but the literature does not support the idea that the reaction energies would be as large as the 60−100 kJ/mol range suggested by the λ_{TOTAL} calculated from experimental $\Delta\nu_{1/2(obs)}$ in Table 3. It appears that the $\Delta\nu_{1/2}$ bandwidth values in Ru polyammine complex melts are actually much smaller than consistent with the energies of the IVCT absorbance bands. The reason(s) for this are unknown. Perhaps there is an unexpectedly narrow distribution of molecular geometries and electron-transfer distances in these semisolid materials.

Last, and arriving at a central observation, the optical electron-transfer barrier for the $Ru(bpy350)_2(CN)_2$ complex melt, 122 kJ/mol, leads by the relation $\lambda_{TOTAL} = E_{OP}/4$, to a predicted thermal barrier for electron transfer of 30 kJ/mol. This value is much smaller than the apparent thermal barrier of 47 kJ/mol in

Table 1, which is consistent with our assignment of control of the latter value by counterion diffusive relocation. As explained above, the thermal barrier for electron transfer is actually a manifestation of the barrier energetics of physical ion motion—the second step in the process of eq 5. In the optical experiment, as the results suggest, the first process, the electron-transfer event in eq 5, is what is monitored. Clearly, the design of semisolid redox materials of any chemical type may be more advanced by attention to improving the dynamics of ionic transport, and/or by the use of even more facile electron-transfer couples than explored here.

Acknowledgment. This research was supported in part by the Department of Energy, Division of Basic Sciences.

Supporting Information Available: Details on spectroelectrochemical cell design and several spectroelectrochemical experiments. This material is available free of charge via the Internet at http://pubs.acs.org.

References and Notes

(1) (a) Velazquez, C. S.; Hutchinson, J. E.; Murray, R. W. *J. Am. Chem. Soc.*, **1993**, *115*, 7896. (b) Poupart, M. W.; Velazquez, C. S.; Hassett, K.; Porat, Z.; Haas, O.; Terrill, R. H.; Murray, R. W. *J. Am. Chem. Soc.* **1994**, *116*, 1165. (c) Kulesza, P. J.; Dickinson, V. E.; Williams, M. E.; Hendrickson, S. M.; Malik, M. A.; Miecznikowski, K.; Murray, R. W. *J. Phys. Chem. B* **2001**, *105*, 5883. (d) Masui, H.; Murray, R. W. *Inorg. Chem.* **1997**, *36*, 5118. (e) Dickinson, V. E.; Masui, H.; Williams, M. E.; Murray, R. W. *J. Phys. Chem. B* **1999**, *103*, 11028. (f) Dickinson, V. E.; Williams, M. E.; Hendrickson, S. M.; Masui, H.; Murray, R. W. *J. Am. Chem. Soc.* **1999**, *121*, 613. (g) Williams, M. E.; Masui, H.; Long, J. W.; Malik, J.; Murray, R. W. *J. Am. Chem. Soc.* **1997**, *199*, 1997. (h) Williams, M. E.; Lyons, L. J.; Long, J. W.; Murray, R. W. *J. Phys. Chem. B* **1997**, *101*, 7584. (i) Williams, M. E.; Crooker, J. C.; Pyati, R.; Lyons, L. J.; Murray, R. W. *J. Am. Chem. Soc.* **1997**, *119*, 10249.

(2) (a) Lee, D.; Hutchinson, J. C.; Leone, A. M.; DeSimone, J. M.; Murrray, R. W. *J. Am. Chem. Soc.* **2002**, *124*, 9310. (b) Lee, D.; Harper, A. S.; DeSimone, J. M.; Murray, R. W. *J. Am. Chem. Soc.* **2003**, *125*, 1096. (c) Harper, A. S.; Lee, D.; Crooker, J. C.; Wang, W.; Williams, M. E.; Murray, R. W. *J. Phys. Chem. B* **2004**, *108*, 1866. (d) Wang, W.; Lee, D.; Leone, A. M.; Murray, R. W. Manuscript in preparation.

(3) Robin, M. B.; Day, P. *Adv. Inorg. Radiochem.* **1967**, *10*, 247.

(4) (a) Marcus, R. A. *J. Chem. Phys.* **1956**, *24*, 966. (b) Marcus, R. A. *J. Chem. Phys.* **1965**, *43*, 58. (c) Marcus, R. A. *Annu. Rev. Phys. Chem.* **1964**, *15*, 155. (d) Marcus, R. A. *Discuss. Faraday Soc.* **1960**, *29*, 21.

(5) (a) Hush, N. S. *Coord. Chem. Rev.* **1985**, *64*, 135. (b) Hush, N. S. *Prog. Inorg. Chem.* **1967**, *8*, 391.

(6) (a) Creutz, C. *Prog. Inorg. Chem.* **1983**, *30*, 1. (b) Crutchley, R. J. *Adv. Inorg. Chem.* **1994**, *41*, 273. (c) Brunschwig, B. S.; Eherson, S.; Sutin, N. *J. Phys. Chem.* **1986**, *90*, 3657. (d) Chen, P.; Meyer, T. J. *Chem. Rev.* **1998**, *98*, 1439. (e) Omberg, K. M.; Chen, P.; Meyer, T. J. *Adv. Chem. Phys.* **1999**, *106*, 553.

(7) (a) Ritchie, J. E.; Murray, R. W. *J. Am. Chem. Soc.* **2000**, *122*, 2964. (b) Ritchie, J. E.; Murray, R. W. *J. Phys. Chem. B* **2001**, *105*, 11523.

(8) Harper, A. S., University of North Carolina, Chapel Hill, Unpublished Results, 2003.

(9) (a) Long, J. W.; Kim, I. K.; Murray, R. W. *J. Am. Chem. Soc.* **1997**, *119*, 11510. (b) Leone, A. M., Ph.D. Thesis, University of North Carolina, Chapel Hill, 2003.

(10) (a) Liu, C. F.; Liu, N. C.; Bailar, J. C. *Inorg. Chem.* **1963**, *3*, 1197. (b) Demas, J. N.; Turner, T. F.; Crosby, G. A. *Inorg. Chem.* **1969**, *8*, 674.

(11) Timpson, C. J.; Bignozzi, C. A.; Sullivan, B. P.; Kober, E. M.; Meyer, T. J. *J. Phys. Chem.* **1996**, *100*, 2915.

(12) Woodard, S. W., Design Consultant, University of North Carolina, Chapel Hill.

(13) Owlia, A.; Wang, Z.; Rusling, J. F. *J. Am. Chem. Soc.* **1989**, *111*, 5091.

(14) Bard, A. J.; Faulkner, L. R. *Electrochemical Methods*: *Fundamental and Applications*, 2nd ed.; John Wiley & Sons: New York, 2001.

(15) (a) Dahms, I. *J. Phys. Chem.* **1968**, *72*, 362. (b) Ruff, I.; Friedrich, V. J. *J. Phys. Chem.* **1971**, *75*, 3297. (c) Majda, M. In *Molecular Design of Electrode Surfaces*; Murray, R. W., Ed.; John Wiley & Sons: New York, 1992.

(16) Lee, D., University of North Carolina, Chapel Hill, Unpublished Results, 2002.

(17) MacCallum, J. R.; Vincent, C. A. *Polymer Electrolyte Reviews*; Elsevier Applied Science: Oxford, UK, 1987; Vol. 1.

(18) (a) Wooster, T. T.; Watanabe, M.; Murray, R. W. *J. Phys. Chem.* **1992**, *96*, 5886. (b) Watanabe, M.; Nagano, S.; Sanui, K.; Ogata, N. *Polym. J.* **1986**, *18*, 809. (c) Watanabe, M.; Itoh, M.; Sanui, K.; Ogata, N. *Macromolecules* **1987**, *20*, 569.

(19) (a) Marcus, R. A.; Sutin, N. *Biochim. Biophys. Acta* **1985**, *811*, 265. (b) Marcus, R. A.; Siddarth, P. In *Photoprocesses in Transition Metal Complexes, Biosystems, and Other Molecules*; Kochanski, E., Ed.; Kluwer Academic Publishers: Dordrecht, The Netherlands, 1992. (c) Sutin, N. *Acc. Chem. Res.* **1982**, *15*, 275. (d) Sutin, N. *Prog. Inorg. Chem.* **1993**, *30*, 441.

(20) (a) Chan, M.-S.; Wahl, A. C. *J. Phys. Chem.* **1978**, *82*, 2542. (b) Young, R. C.; Keene, F. R.; Meyer, T. J. *J. Am. Chem. Soc.* **1977**, *99*, 2468. (c) Brown, G. M.; Sutin, N. J. *J. Am. Chem. Soc.* **1979**, *101*, 883. (d) Brown, G. M.; Krentzien, H. J.; Abe, M.; Taube, H. *Inorg. Chem.* **1979**, *18*, 3374.

(21) Marcus, R. A. *J. Phys. Chem. B* **1998**, *102*, 10071.

(22) Taking k_{EX} and D_{ClO_4} values from Table 1, "*a*" can be calculated. If K_{EQ} is assumed to be 1, then the calculated "*a*" values are 13 to 15 Å; if K_{EQ} is 30% (i.e. 0.3), then, "*a*" ranges from 7 to 8 Å.[2a]

(23) (a) The peak at 6900 cm^{-1} is attributed to $Ru^{3+}-CN-Ru^{2+}$ polymeric species. For −CN− bridged Ru polynuclear species, IVCT bands are observed at ∼7200 (trinuclear) and 7700 (binuclear) cm^{-1} in acetonitrile.[23b] Such polymeric species are formed as an impurity during the synthesis of the $Ru(bpy)_2(CN)_2$ complex.[23c] Such polynuclear species are also known to have very high extinction coefficient values (>10 000 M^{-1} cm^{-1}), so it is not surprising that a small amount of the polymeric species results in a peak with high absorbance. (b) Bignozzi, C. A.; Argazzi, R.; Schoonover, J. R.; Gordon, K. C.; Dyer, R. B.; Scandola, F. *Inorg. Chem.* **1992**, *31*, 5260. (c) Bignozzi, C. A.; Scandola, F. *Inorg. Chim. Acta* **1984**, *86*, 133.

(24) The values are approximate because (a) the exact path length and concentration of the absorbing species are not known and (b) the maximum absorbance is not a steady-state absorbance. ϵ was estimated by assuming a path length of 50 μm defined by the spacer, the concentration was assumed to be one-third of the total concentration, and the absorbance value is obtained from a curve fit; the electronic coupling term was calculated by using the reported equations.[6]

(25) Hupp, J. T.; Dong, Y.; Blackbourn, R. L.; Lu, H. *J. Phys. Chem.* **1993**, *97*, 3278.

(26) Williams, M. E.; Masui, H.; Murray, R. W. *J. Phys. Chem. B* **2000**, *104*, 10699.

(27) (a) Lewis, N. A.; Yaw, O. *J. Am. Chem. Soc.* **1988**, *110*, 2307. (b) Lewis, N. A.; Yaw, O. S.; Purcell, W. L. *Inorg. Chem.* **1989**, *28*, 3796. (c) Lewis, N. A.; Yaw, O. S *J. Am. Chem. Soc.* **1989**, *111*, 7624. (d) Chang, J. P.; Fung, E. Y.; Curtis, J. C. *Inorg. Chem.* **1986**, *25*, 4233. (e) Kuznetzov, A. M.; Phelps, D. K.; Weaver, M. J. *Int. J. Chem. Kinet.* **1990**, *22*, 815. (f) Blackbourn, R. L.; Hupp, J. T. *Chem. Phys. Lett.* **1988**, *150*, 399. (g) Blackbourn, R. L.; Hupp, J. T. *J. Phys. Chem.* **1990**, *94*, 1788. (h) Blackbourn, R. L.; Dong, Y.; Lyon, A.; Hupp, J. T. *Inorg. Chem.* **1994**, *33*, 4446.